NANO LETTERS

LETTER

pubs.acs.org/NanoLett

Toward Wafer Scale Fabrication of Graphene Based Spin Valve Devices

Ahmet Avsar,[∇,†] Tsung-Yeh Yang,[∇,‡,§] Sukang Bae,[∇,∥] Jayakumar Balakrishnan,[†] Frank Volmer,[‡,§] Manu Jaiswal,[†] Zheng Yi,[†,∥] Syed Rizwan Ali,[‡,§] Gernot Güntherodt,[‡,§] Byung Hee Hong,[*,∥] Bernd Beschoten,[*,‡,§] and Barbaros Özyilmaz[*,†,⊥,#]

[†]Graphene Research Center & Department of Physics, National University of Singapore, 2 Science Drive 3, Singapore 117542, Singapore

[‡]II. Institute of Physics, RWTH Aachen University, 52074 Aachen, Germany

[§]JARA: Fundamentals of Future Information Technology, Jülich-Aachen Research Alliance, Aachen, Germany

[∥]SKKU Advanced Institute of Nanotechnology (SAINT) and Center for Human Interface Nanotechnology (HINT), Department of Chemistry, Sungkyunkwan University, Suwon, 440-746, Korea

[⊥]Nanocore, National University of Singapore, Faculty of Engineering, Engineering Block A, EA, Level 4, Room No.27, Singapore 117576, Singapore

[#]NUS Graduate School for Integrative Sciences and Engineering (NGS), 05-01, 28 Medical Drive, Singapore 117456, Singapore

Supporting Information

ABSTRACT: We demonstrate injection, transport, and detection of spins in spin valve arrays patterned in both copper based chemical vapor deposition (Cu-CVD) synthesized wafer scale single layer and bilayer graphene. We observe spin relaxation times comparable to those reported for exfoliated graphene samples demonstrating that chemical vapor deposition specific structural differences such as nanoripples do not limit spin transport in the present samples. Our observations make Cu-CVD graphene a promising material of choice for large scale spintronic applications.

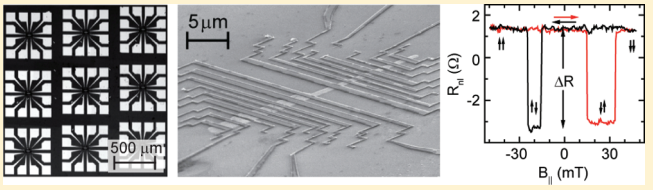

KEYWORDS: Spin transport, Hanle precession, graphene, CVD growth, ripple

High charge mobility,[1] small spin−orbit coupling,[2] negligible hyperfine interaction,[3] the electric field effect,[4] and last but not least the ability to sustain large current densities[5] make graphene an exceptional material for spintronic applications. The demonstration of micrometer long spin relaxation length in exfoliated single layer graphene (SLG) and bilayer graphene (BLG) even at room temperature (RT)[6−12] and spin relaxation times in the order of nanoseconds[11,12] may pave the way to realize several of the recently proposed spin-based device concepts.[13−15] However, for realistic device applications it remains to be seen, if such impressive spin transport properties can also be achieved in wafer scale chemical vapor deposition (CVD) graphene. Equally important, spin transport studies based on micromechanically exfoliated graphene sheets are often too slow for the quick exploration of the basic spin properties of graphene and for testing potential device architectures. The recent progress in the Cu-based CVD (Cu-CVD) growth of graphene has a strong impact on charge-based graphene device applications.[16] However, CVD graphene has a large number of structural differences when compared to exfoliated graphene such as grain boundaries,[17] defects like pentagons, heptagons, octagons, vacancies, 1D line charges,[18] and in the case of bilayer graphene possibly interlayer stacking faults.[19,20] In addition, the current growth and transfer process introduces residual catalysts, wrinkles, quasi-periodic nanoripple arrays, and new classes of organic residues.[19] Despite all of these defects, charge mobilities in CVD graphene field effect transistors (FETs) have been comparable to what has been reported for most exfoliated graphene FETs on Si/SiO_2 substrates.[21] Whether this synthesis route will also play an important role for spin transport studies and large scale spin-based device applications depends on how the same defects affect the spin relaxation times.

In this Letter, we demonstrate spin transport in Cu-CVD grown SLG and BLG transferred onto conventional Si/SiO_2 substrates and discuss the role of nanoripples, a ubiquitous surface structure of Cu-CVD graphene.[19] The growth and transfer of large-scale Cu-CVD graphene are the same as in ref 17. By controlling the postgrowth annealing time of CVD graphene, we can obtain films with SLG coverage up to 95% or additional BLG coverage up to 40%. The latter samples are ideal for directly comparing spin transport in both systems. The inset in Figure 1a shows the optical image of CVD SLG and BLG on a Si/SiO_2 substrate. Raman spectra (Figure 1a) with insignificant D-band peak near 1400 cm^{-1} show the high quality of both single-layer and A−B stacked bilayer samples. Spin valves are fabricated by first forming isolated SLG and BLG stripes by means of a PMMA etch mask. A second e-beam lithography step is used to form the device electrodes. Next, we deposit in the same run a ∼2 nm

Received: March 3, 2011
Revised: April 25, 2011
Published: May 12, 2011

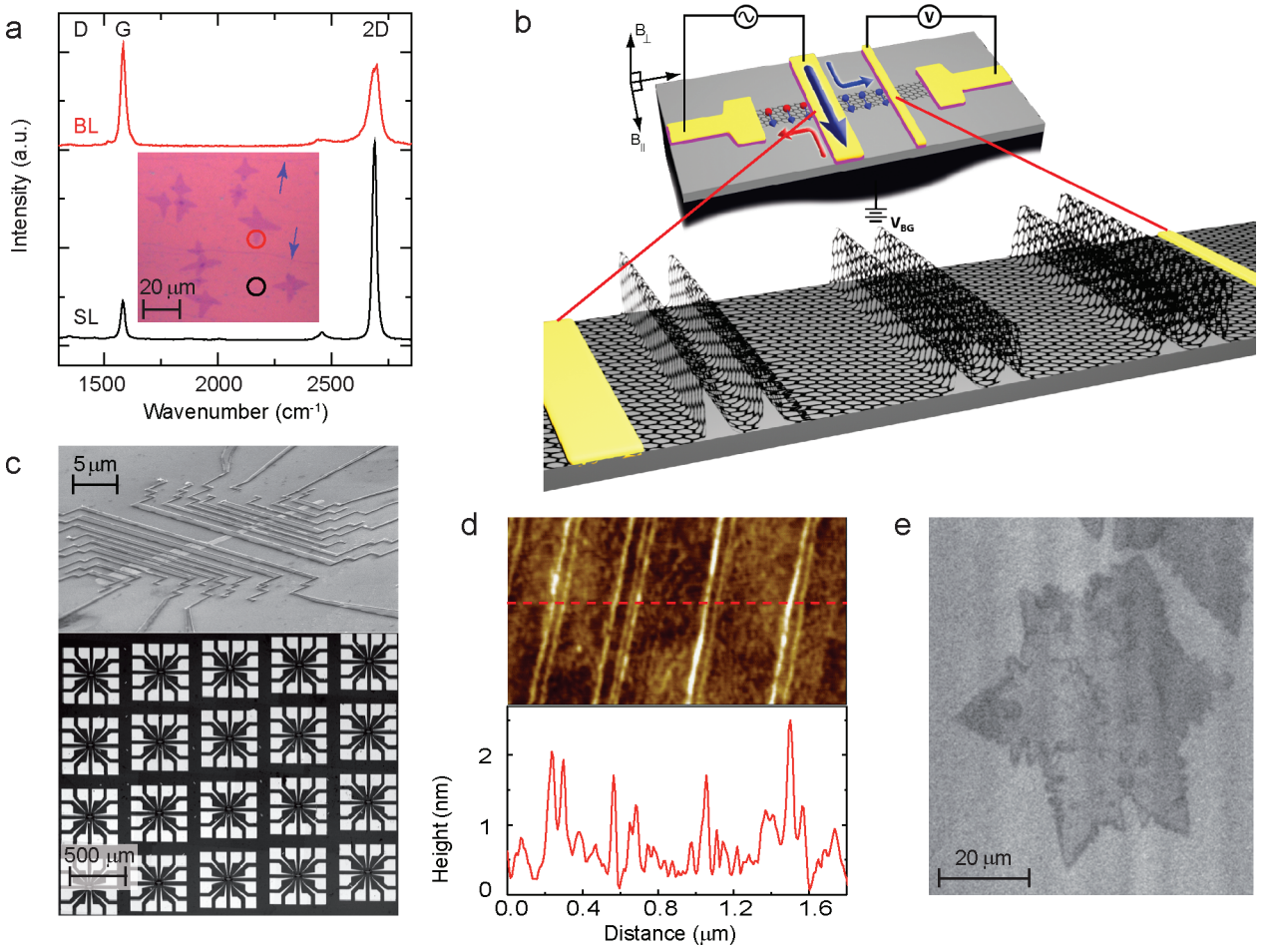

Figure 1. (a) Optical image of CVD single and bilayer graphene on Si/SiO_2 substrate (300 nm SiO_2 thickness) with their respective Raman spectra. Black and red circles indicate the Raman spectroscopy locations. Blue arrows point to low density wrinkles typical for CVD graphene films. (b) Schematics for a graphene based nonlocal spinvalve together with a possible configuration of quasi-periodic nanoripples in a spin valve. (c) Bottom: Optical image of a 5 × 5 device array. CVD graphene allows the fabrication of large arrays of identical lateral spin valves. Top: Scanning electron micrograph of CVD SLG spin sample with multiple nonlocal spin valve devices. Electrode widths range from 0.3 to 1.2 μm. (d) High-resolution contact mode AFM image of CVD graphene after transfer onto Si/SiO_2 wafer revealing the presence localized nanoscale ripples of high density. (e) SEM image of submonolayer graphene coverage on Cu.

thick MgO layer followed by 35 nm thick Co electrodes; details are discussed elsewhere.[11] This approach allows the batch fabrication of large arrays of lateral spin valves with a fast turn-around time well suited for studying device physics. An optical image of a 5 × 5 array of such devices is shown in Figure 1c (lower panel) together with a scanning electron microscopy (SEM) image (Figure 1c (upper panel)) of multiple spin valve junctions showing the specific electrode configuration at a single site. The typical length and width of the spin channel in our spin valve devices are in the range of 1−2 μm. Measurements are performed with standard ac lock-in techniques at low frequencies using the local four terminal setup for charge conductivity measurements and the nonlocal setup for spin transport measurements.[22] The schematic of the nonlocal setup is shown in Figure 1b. The spin transport results obtained from CVD graphene are compared with the results from exfoliated graphene samples of similar charge mobilities prepared under identical conditions (see Supporting Information).

Prior to any spin transport measurements, we characterized the conductivity of our devices as a function of back gate voltage at RT and at 5 K. Panels a and f of Figure 2 show the typical ambipolar field effect in our CVD SLG and BLG devices, respectively. A weak electron doping, possibly resulting from the MgO barrier, is observed in all our devices ($V_{\text{Charge Neutrality Point}} \approx -5$ V, not shown). In addition, our spin valves show a strong asymmetry between the electron ($n > 0$) and hole ($n < 0$) doped region, such that the conductance in the hole region is strongly distorted.[23] Here, we limit our spin transport analysis mainly to the electron-doped region. In total, we have measured spin transport across 15 CVD SLG and BLG nonlocal spinvalve junctions. Field effect mobilities $\mu = \Delta\sigma/(e\Delta n)$ are extracted at $n \approx 2 \times 10^{12}/\text{cm}^2$, and vary from 1000 to 2100 $\text{cm}^2/(\text{V s})$. Here we discuss representative CVD SLG junctions and BLG junctions with mobilities of ≈1400 and ≈2100 $\text{cm}^2/(\text{V s})$, respectively. These values are similar to the values reported for most of the exfoliated graphene based spin valves in the literature.[6−12] Therefore, this allows a direct comparison of the spin transport properties of CVD graphene with exfoliated graphene.

We first discuss RT spin transport results in CVD SLG near the charge neutrality point (CNP). Sweeping the in-plane magnetic field $B_{\|}$ (Figure 1b) changes the relative magnetization directions of the Co electrodes and hence the spin accumulation

dx.doi.org/10.1021/nl200714q |*Nano Lett.* 2011, 11, 2363–2368

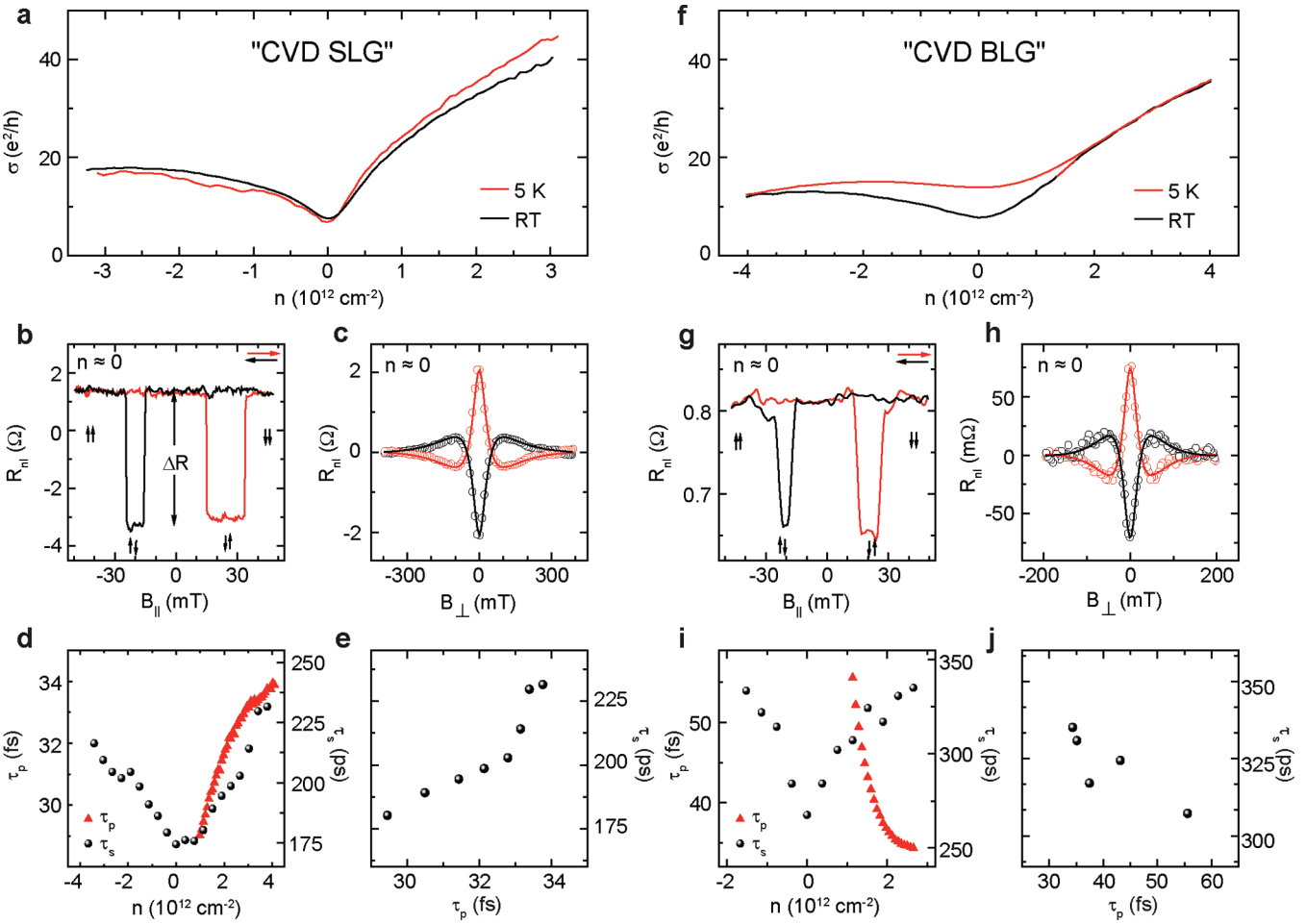

Figure 2. (a) Conductivity of CVD SLG at RT and at $T = 5$ K as a function of carrier density with a strong asymmetry between electron and hole-doped region. (b) Bipolar spin signal obtained near the charge neutrality point. (c) Hanle spin precession measurement confirms the spin signal in (b). (d) Both τ_s and τ_p increase with increasing electron carrier density. (e) Linear dependence of τ_s and τ_p showing that EY-like spin scattering is dominant in CVD SLG. (f) Conductivity of CVD BLG at RT and at $T = 5$ K as a function of carrier density. (g and h) Spin valve and spin precession measurements in CVD BLG, respectively. (i) Electron carrier density dependence of τ_s and τ_p at RT. (j) Scaling of τ_s with τ_p indicates DP type spin scattering as the dominant spin scattering mechanism in CVD BLG.

between the injector and detector electrodes. This leads to a clear bipolar nonlocal spin signal with a change in resistance of $\Delta R \approx 4$ Ω (Figure 2b). The origin of the spin signal is confirmed by conventional Hanle spin precession measurements.[24] For this purpose, the magnetizations of the electrodes are first aligned parallel (antiparallel) to each other by the in-plane magnetic field $B_{\|}$. This is followed by a magnetic field $B_{\perp}$ perpendicular to the graphene plane forcing the spins to precess about the latter (Figure 2c). As expected, this also yields $\Delta R \approx 4$ Ω. With $L \approx 1.15$ μm being the separation between the electrodes (center-to-center distance) and ω_L the Larmor frequency, we fit our data by

$$R_{nl} \propto \int_0^{\infty} \frac{1}{\sqrt{4\pi D_s t}} \exp\left(\frac{-L^2}{4D_s t}\right) \exp\left(\frac{-t}{\tau_s}\right) \cos(\omega_L t)\, dt \quad (1)$$

This gives a transverse spin relaxation time of $\tau_s \approx 180$ ps, a spin diffusion constant of $D_s \approx 0.007$ m^2/s, and, hence, a spin relaxation length $(\lambda_s = (D_s \tau_s)^{1/2})$ of $\lambda_s \approx 1.1$ μm. A clear spin valve signal is also observed in the CVD BLG samples (Figure 2g). The origin of the signal is again confirmed by the Hanle measurements (Figure 2h). Using the same fitting procedure as for the SLG measurements, we obtain for the BLG a spin relaxation time $\tau_s \approx 285$ ps, a spin diffusion constant of $D_s \approx 0.0063$ m^2/s, and, hence, a spin relaxation length of $\lambda_s \approx 1.35$ μm.

Next, we determine the dominant spin scattering mechanisms in CVD SLG and BLG by evaluating the functional dependence of τ_s on the momentum scattering time τ_p. For the Elliott−Yafet (EY) mechanism, spin dephasing occurs during momentum scattering. Therefore, the spin relaxation time is directly proportional to the momentum scattering time $(\tau_s \propto \tau_p)$.[25] On the other hand, the D'yakonov−Perel' (DP) mechanism refers to the case where spin dephasing takes place between momentum scattering events, which may result from random Bychkov−Rashba-like spin−orbit fields.[26] This leads to a spin relaxation time, which is inversely proportional to the momentum scattering time $(\tau_s \propto \tau_p^{-1})$.[27] Away from the CNP, the electric field effect in graphene provides a convenient tool to correlate τ_s and τ_p.[9,28] Provided that *both* quantities show a discernible charge density dependence, such a correlation can be used to identify the limiting spin dephasing mechanism as has been demonstrated for exfoliated graphene samples.[11] Using this

dx.doi.org/10.1021/nl200714q |*Nano Lett.* 2011, 11, 2363–2368

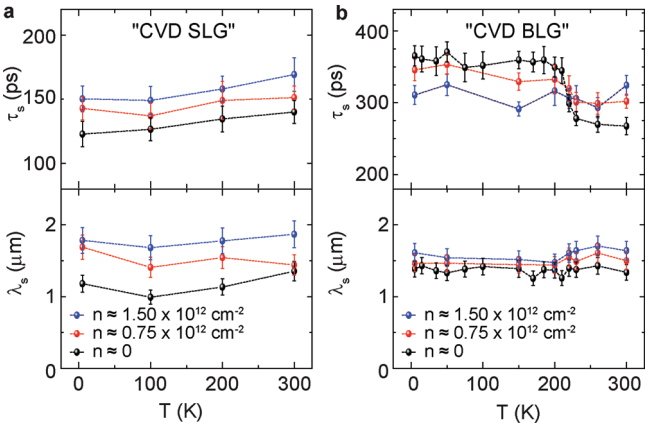

Figure 3. (a) T dependent τ_s and λ_s are shown for CVD SLG for three different electron carrier densities. (b) The T dependences of τ_s have different behavior for different doping levels in CVD BLG. λ_s depends very weakly on T, but its n dependence is much weaker than for CVD SLG. λ_s is observed to be very weakly dependent on temperature for fixed carrier densities in both CVD SLG and BLG, since different temperature dependence trends of τ_s and D_s almost suppress each other in both systems (see Supporting Information).

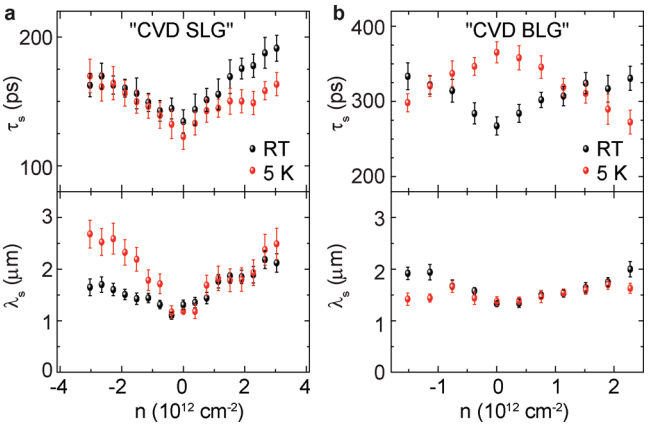

Figure 4. (a) Charge carrier density dependence of τ_s and λ_s at RT and at 5 K for CVD SLG. (b) Charge carrier density dependence of τ_s and λ_s at RT and 5 K for CVD BLG. Note that the carrier density dependence of τ_s of CVD BLG at 5 K shows an opposite trend compared to RT.

approach at RT, the dominant spin scattering mechanism for exfoliated SLG spin valves with spin injection through leaky contacts has been identified to be of EY type.[7,9] In exfoliated BLG, the DP type mechanism is dominant.[11]

We start our discussion of the CVD graphene with the SLG case and note that τ_s increases with doping by ~35% from 175 to 230 ps in typical gate bias ranges. The n dependence of τ_p within the Boltzmann transport theory framework[28] is extracted from

$$\tau_p(n) = \frac{h\sigma}{e^2 v_F(\sqrt{n g_s g_v \pi})}$$

(Figure 2d), where g_v and g_s are the 2-fold valley and spin degeneracies, respectively, h is Planck's constant, e is the electron charge, and v_F is the Fermi velocity. Combining both results we obtain an approximately linear scaling of τ_s with τ_p, i.e. ($\tau_s \propto \tau_p$) (Figure 2e). In the case of CVD BLG, τ_s increases with increasing n from 265 to 335 ps. However, τ_p shows a *decreasing* trend with increasing n as extracted from $\tau_p = m^*\sigma/e^2 n$, where m^* is the effective mass of the charge carriers (Figure 2i).[29] Therefore, correlating τ_s and τ_p, we obtain for BLG an inverse scaling (Figure 2j), i.e., ($\tau_s \propto \tau_p^{-1}$). These results summarize the key findings of our experiments: At RT, the typical spin parameters in CVD graphene differ neither quantitatively nor qualitatively from exfoliated graphene: τ_s, D_s, and λ_s are of the same order of magnitude in both systems.[6−12] Equally important, their charge density dependence qualitatively remains the same as exfoliated samples.[7,9,11] Hence, the limiting spin dephasing mechanisms at RT remain EY type and DP type in CVD SLG and CVD BLG, respectively.

These results are at first rather surprising, since CVD graphene has additional solvent residues,[30] and structural differences,[18] in particular grain boundaries,[17] when compared to exfoliated graphene. Also, Cu-CVD growth typically requires high temperatures of 1000−1050 °C. This leads to single-crystal terraces and step edges in Cu, which in turn give rise to additional nanoripples in graphene after transfer (inset Figure 1b). They are best seen in high-resolution contact mode AFM images after being transferred onto Si/SiO_2 substrates (Figure 1d). Such (double) peak structures of 0.2−2 nm in height, ~100 nm in width, and ~300 nm separation are quasi-periodic across an area (≥10 μm^2) much larger than the actual spin valve size.[19] Assuming for example a channel area of ~1 × 1 μm^2, there will be approximately three such features present independent of their relative orientations with respect to the ferromagnetic electrodes. Thus, the growth and transfer processes cause local curvature in graphene which may affect spin−orbit coupling. In carbon nanotubes (CNTs), local curvature has been shown to strongly enhance spin−orbit coupling.[2,31] However, it is important to note that the radius of curvatures in CNT and our samples differ greatly. The average radius of curvature in quasi-periodic nanoripples is ~200 nm, which leads to a much weaker spin−orbit coupling strength of ~3 μeV (Supporting Information). A comparison with the intrinsic spin−orbit coupling of graphene (~24 μeV)[32] suggests that the nanoripples in the present samples cannot set a limit for spin transport. The high-temperature growth of graphene on the Cu surface does however have one advantage. The rather weak interaction with the underlying Cu substrates allows graphene to grow continuously crossing atomically flat terraces, step edges, and vertices without introducing defects.[33] Thus, by controlling pregrowth annealing[16] and fine-tuning growth parameters,[34] it is now possible to synthesize Cu-CVD graphene with submillimeter grain size. The grain size of our Cu-CVD graphene is ~50−100 μm, as determined by SEM of submonolayer coverage graphene on the Cu foil (Figure 1e). This makes spin transport across grain boundaries in submicrometer size spin valves highly unlikely. Thus, under current growth conditions, neither grain boundaries nor nanoripples, which are the two key differences of Cu-CVD graphene with respect to exfoliated graphene, have a limiting effect on spin transport. The main spin scattering mechanism in Cu-CVD samples seems to originate from the same source as in the case of spin valves based on exfoliated samples: adatoms,[35] scattering from the tunneling barrier interface,[36] and the supporting substrate.[26]

Last but not least, we present spin transport measurements as a function of temperature from RT down to 5 K (Figure 3). The temperature dependence of τ_s, λ_s, and D_s has been measured for three distinct doping levels: (1) at the CNP,

dx.doi.org/10.1021/nl200714q |*Nano Lett.* 2011, 11, 2363–2368

(2) at $n \approx 7.5 \times 10^{11}/\mathrm{cm}^2$, and (3) at $n \approx 1.5 \times 10^{12}/\mathrm{cm}^2$. We focus our discussion on the quantity τ_s. In CVD SLG spin valves, similar to results in exfoliated SLG devices,[11] we observe at all doping levels only a weak temperature dependence (Figure 3a). The CVD BLG, on the other hand, shows a more complex temperature dependence of τ_s, which differs strongly between the CNP and the high carrier densities (Figure 3b). At high doping, τ_s in CVD BLG is only weakly temperature dependent. However, at the CNP τ_s shows a sharp increase from 260 to 360 ps between 250 and 200 K. In contrast, for temperatures above 250 K and below 200 K, τ_s varies again only weakly with temperature at the CNP. This nonmonotonic temperature dependence at the CNP is typical also for our exfoliated bilayer devices.[11] Finally, we discuss the n dependence of τ_s and λ_s in CVD samples at 5 K. Similar to the RT case, at low temperature (LT) τ_s increases with increasing n in SLG (Figure 4a). This implies that in SLG the main spin scattering mechanism remains the EY type even at LT. However, in CVD BLG, τ_s decreases with increasing n in contrast to RT (Figure 4b). This behavior becomes noticeable for temperatures below 200 K but is most pronounced at the lowest measured temperature ($T = 5$ K). While this qualitative change of the charge density dependence of τ_s at low temperature is not yet understood, it is bilayer specific. A very similar behavior has also been observed previously in exfoliated BLG samples.[11,12] Thus, comparing our CVD graphene results with results obtained in exfoliated graphene spin valves, we conclude that the temperature and the carrier density dependence of τ_s are comparable in both systems.

In conclusion, we have demonstrated spin injection, spin transport, and spin detection in Cu-CVD SLG and BLG samples. The key spin transport parameters such as τ_s and λ_s have been measured as a function of charge carrier density and temperature. They are comparable to what has been already reported in both exfoliated SLG and exfoliated BLG samples making Cu-CVD graphene a promising candidate for possible large scale spintronic applications. We have also discussed the importance of Cu-CVD graphene specific quasi-periodic arrays of nanoripples in spin transport. While in current samples the local curvature is too small to enhance the spin−orbit coupling significantly, such quasi-periodic nanoripple arrays may provide intriguing opportunities in controlling spin currents through spin−orbit coupling due to local curvature and local strain.

■ ASSOCIATED CONTENT

Ⓢ Supporting Information. Additional information on carrier density dependence of spin signal, spin diffusion constant, and spin injection efficiency in CVD single layer graphene and bilayer graphene, carrier density dependence of conductivity, spin relaxation time, and spin relaxation length in exfoliated single layer graphene and bilayer graphene, and estimate of the nanoripple induced spin−orbit coupling strength. This material is available free of charge via the Internet at http://pubs.acs.org.

■ AUTHOR INFORMATION

Corresponding Author

*E-mail: barbaros@nus.edu.sg, bernd.beschoten@physik.rwth-aachen.de, byunghee@skku.edu.

Author Contributions

▽These authors contributed equally to this work.

■ ACKNOWLEDGMENT

This work is supported by the Singapore National Research Foundation Grants NRF-RF2008-07 and NRF-CRP (R-143-000-360-281), by a NUS/SMF horizon grant, by the US Office of Naval Research (ONR and ONR Global), by NUS NanoCore, by DFG through FOR 912, by NUS Young Investigator Award, by JARA-FIT, and by the National Research Foundation of Korea (NRF) funded by the Ministry of Education, Science and Technology (2010-0028075, 2010-0081966, 2011-0006268).

■ REFERENCES

(1) Bolotin, K. I.; Sikes, K. J.; Jiang, Z.; Klima, M.; Fudenberg, G.; Hone, J.; Kim, P.; Stormer, H. L. *Solid State Commun.* **2008**, *146*, 351–355.
(2) Huertas-Hernando, D.; Guinea, F.; Brataas, A. *Phys. Rev. B* **2006**, *74*, 155426.
(3) Trauzettel, B.; Bulaev, D. V.; Loss, D.; Burkard, G. *Nat. Phys.* **2007**, *3*, 192–196.
(4) Novoselov, K. S.; Geim, A. K.; Morozov, S. V.; Jiang, D.; Zhang, Y.; Dubonos, S. V.; Grigorieva, I. V.; Firsov, A. A. *Science* **2004**, *306*, 666–669.
(5) Geim, A. K. *Science* **2009**, *324*, 1530–1534.
(6) Tombros, N.; Jozsa, C.; Popinciuc, M.; Jonkman, H. T.; van Wees, B. J. *Nature* **2007**, *448*, 571–574.
(7) Popinciuc, M.; Józsa, C.; Zomer, P. J.; Tombros, N.; Veligura, A.; Jonkman, H. T.; van Wees, B. J. *Phys. Rev. B* **2009**, *80*, 214427.
(8) Han, W.; Pi, K.; Bao, W.; McCreary, K. M.; Yan, L.; Wang, W. H.; Lau, C. N.; Kawakami, R. K. *Appl. Phys. Lett.* **2009**, *94*, 222109.
(9) Józsa, C.; Maassen, T.; Popinciuc, M.; Zomer, P. J.; Veligura, A.; Jonkman, H. T.; van Wees, B. J. *Phys. Rev. B* **2009**, *80*, 241403.
(10) Shiraishi, M.; Ohishi, M.; Nouchi, R.; Mitoma, N.; Nozaki, T.; Shinjo, T.; Suzuki, Y. *Adv. Funct. Mater.* **2009**, *19*, 3711–3716.
(11) Yang, T. Y.; Balakrishnan, J.; Volmer, F.; Avsar, A.; Jaiswal, M.; Samm, J.; Ali, S. R.; Pachoud, A.; Zeng, M.; Popinciuc, M.; Güntherodt, G.; Beschoten, B.; Özyilmaz, B. *ArXiv:1012.1156v1*, 2010.
(12) Han, W.; Kawakami, R. K. *ArXiv:1012.3435v2*, 2010.
(13) Koo, H. C.; Kwon, J. H.; Eom, J.; Chang, J.; Han, S. H.; Johnson, M. *Science* **2009**, *325*, 1515–1518.
(14) Michetti, P.; Recher, P.; Iannaccone, G. *Nano Lett.* **2010**, *10*, 4463−4469
(15) Dery, H.; Wu, H.; Ciftcioglu, B.; Huang, M.; Song, Y.; Kawakami, R.; Shi, J.; Krivorotov, I.; Zutic, I.; Sham, L. J. *ArXiv:1101.1497*, 2011.
(16) Bae, S.; Kim, H.; Lee, Y.; Xu, X.; Park, J. S.; Zheng, Y.; Balakrishnan, J.; Lei, T.; Kim, H. R.; Song, Y.; Kim, Y. J.; Sim, K. S.; Özyilmaz, B.; Ahn, J. H.; Hong, B. H.; Iijima, S. *Nat. Nanotechnol.* **2010**, *5*, 574–578.
(17) Li, X. S.; Cai, W.; An, J.; Kim, S.; Nah, J.; Yang, D.; Piner, R.; Velamakanni, A.; Jung, I.; Tutuc, E.; Banerjee, S. K.; Colombo, L.; Ruoff, R. S. *Science* **2009**, *324*, 1312–1314.
(18) Ferreira, A.; Xu, X.; Tan, C. L.; Bae, S.; Peres, N. M. R.; Hong, B. H.; Özyilmaz, B.; Castro Neto, A. H.; *Europhys. Lett.* **2011**, *94*, 28003.
(19) Zheng, Y.; Ni, G. X.; Bae, S.; Tan, C. L.; Toh, C. T.; Kim, H. R.; Im, D.; Ahn, J. H.; Hong, B. H.; Özyilmaz, B. 2010, Submitted.
(20) Lee, S.; Lee, K.; Zhong, Z. *Nano Lett.* **2010**, *10*, 4702–4707.
(21) Li, X. S.; Magnuson, C. W.; Venugopal, A.; An, J.; Suk, J. W.; Han, B.; Borysiak, M.; Cai, W.; Velamakanni, A.; Zhu, Y.; Fu, L.; Vogel, E. M.; Voelkl, E.; Colombo, L.; Ruoff, R. S. *Nano Lett.* **2010**, *10*, 4328–4334.
(22) Jedema, F. J.; Filip, A. T.; van Wees, B. J. *Nature* **2001**, *410*, 345–348.
(23) Nouchi, R.; Tanigaki, K. *Appl. Phys. Lett.* **2010**, *96*, 253503.
(24) Jedema, F. J.; Heersche, H. B.; Filip, A. T.; Baselmans, J. J. A.; van Wees, B. J. *Nature* **2002**, *416*, 713–716.

(25) Elliott, R. J. *Phys. Rev.* **1954**, *96*, 266–279.
(26) Ertler, C.; Konschuh, S.; Gmitra, M.; Fabian, J. *Phys. Rev. B* **2009**, *80*, 041405.
(27) D'yakonov, M. I.; Perel', V. I. *Sov. Phys. Solid State* **1972**, *13*, 3023–3026.
(28) Tan, Y.-W.; Zhang, Y.; Bolotin, K.; Zhao, Y.; Adam, S.; Hwang, E. H.; Das Sarma, S.; Stormer, H. L.; Kim, P. *Phys. Rev. Lett.* **2007**, *99*, 246803.
(29) Monteverde, M.; Ojeda-Aristizabal, C.; Weil, R.; Bennaceur, K.; Ferrier, M.; Guéron, S.; Glattli, C.; Bouchiat, H.; Fuchs, J. N.; Maslov, D. L. *Phys. Rev. Lett.* **2010**, *104*, 126801.
(30) Heo, J.; Chung, H. J.; Lee, S. H.; Yang, H.; Seo, D. H.; Shin, J. K.; Chung, U.; Seo, S.; Hwang, E. M.; Das Sarma, S. *ArXiv:1009.2506*, 2010.
(31) Kuemmeth, F.; Ilani, S.; Ralph, D. C.; McEuen, P. L. *Nature* **2008**, *452*, 448–452.
(32) Gmitra, M.; Konschuh, S.; Ertler, C.; Ambrosch-Draxl, C.; Fabian, J. *Phys. Rev. B* **2009**, *80*, 235431.
(33) Wofford, J. M.; Nie, S.; McCarty, K. F.; Bartelt, N. C.; Dubon, O. D. *Nano Lett.* **2010**, *10*, 4890–4896.
(34) Li, X. S.; Magnuson, C. W.; Venugopal, A.; Vogel, E. M.; Ruoff, R. S.; Colombo, L. *ArXiv:1010.3903v1*, 2010.
(35) Castro Neto, A. H.; Guinea, F. *Phys. Rev. Lett.* **2009**, *103*, 026804.
(36) Han, W.; Pi, K.; McCreary, K. M.; Li, Y.; Wong, J. J. I.; Swartz, A. G.; Kawakami, R. K. *Phys. Rev. Lett.* **2010**, *105*, 167202.